1989

Effects of an Embedded Vortex on Injectant from a Single Film-Cooling Hole in a Turbulent Boundary Layer

Ligrani, P.M.; William, W.

ASME

Ligrani, P. M., and W. Williams. "Effects of an embedded vortex on injectant from a single film-cooling hole in a turbulent boundary layer." ASME 1989 International Gas Turbine and Aeroengine Congress and Exposition. American Society of Mechanical Engineers, 1989.

https://hdl.handle.net/10945/62169

THE AMERICAN SOCIETY OF MECHANICAL ENGINEERS
345 E. 47 St., New York, N.Y. 10017

89-GT-189

Effects of an Embedded Vortex on Injectant from a Single Film-Cooling Hole in a Turbulent Boundary Layer

P. M. LIGRANI*, W. WILLIAMS+
Department of Mechanical Engineering
Naval Postgraduate School
Monterey, California 93943-5000

ABSTRACT

Effects of embedded longitudinal vortices on heat transfer in turbulent boundary layers with injection from a single film cooling hole are described. These results were obtained at a freestream velocity of 10 m/s, with a film cooling hole inclined 30 degrees to horizontal and a blowing ratio of about 0.50. The ratio of vortex core diameter to injection hole diameter was 2.14, and the ratio of circulation to injection velocity times hole diameter was about 2.8. Coolant distributions and spatially resolved heat transfer measurements indicate that injection hole centerlines must be a least 2.0 - 2.5 vortex core diameters away from the vortex center in the lateral direction to avoid significant alterations to wall heat transfer and distributions of film coolant. Under these circumstances, protection from film cooling is evident at least up to 55 hole diameters downstream of injection. When the injection hole is closer to the vortex center, secondary flows convect most injectant into the vortex upwash and thermal protection from film cooling is destroyed for streamwise locations from the injection hole greater than 17.5 hole diameters.

NOMENCLATURE

c - average vortex core radius in spanwise direction

d - injection hole diameter

h - heat transfer coefficient $\dot{q}_w''/(T_{r\infty} - T_w)$

m - blowing ratio, $\rho_c U_c / \rho_\infty U_\infty$

$\dot{q}''$ - heat flux

St - Stanton number

St_o - baseline Stanton number, no film cooling, no vortex

St_f - Stanton number with film cooling only

T - static temperature

U - mean velocity

x - downstream distance as measured from the leading edge of the boundary layer trip or from the downstream edges of injection holes when used as x/d

y - vertical distance from the test surface upward

z - spanwise distance from the test section center line

ξ - unheated starting length

ρ - density

θ - non-dimensional coolant temperature, $(T_{rc} - T_{r\infty})/(T_w - T_{r\infty})$

δ_1 - boundary layer displacement thickness

Γ - circulation of streamwise vorticity

subscripts

c - coolant at exit of injection holes

r - recovery condition

w - wall

* Associate Professor +Graduate Student

Presented at the Gas Turbine and Aeroengine Congress and Exposition—June 4-8, 1989—Toronto, Ontario, Canada
This paper has been accepted for publication in the Transactions of the ASME
Discussion of it will be accepted at ASME Headquarters until September 30, 1989

y - normal direction

z - spanwise direction

∞ - freestream

INTRODUCTION

Film cooling is used as a means to protect surfaces from the thermal loading which results from exposure to hot gases. However, distributions of coolant and the resulting thermal protection are often disturbed by secondary flows. This is especially true for turbine passages. Here, embedded vortices, in particular, cause perturbations which often lead to local hot spots at locations where film cooling would ordinarily be expected to provide adequate protection, and where protection is most needed. Such vortices originate from the centrifugal instability resulting from concave curvature, as well as from local pressure gradients which exist at locations such as the intersection between the blade and endwall.

Studies of the interactions between embedded vortices and wall injection for gas turbine application are relatively scarce. One of the earliest is reported by Blair (1974), who measured heat transfer on an endwall film-cooled using a slot inclined at a 30 degree angle. The large vortex located in the corner between the endwall and the suction surface of their cascade was believed to cause significant variations of measured heat transfer and film cooling effectiveness. Experimental studies on the influence of the endwall on film cooling from blades using one and two rows of injection holes were performed by Goldstein and Chen (1985,1987). These investigators found a triangular region which exists on the convex side of the blade where coolant is swept away from the surface by the passage vortex. In contrast, the concave side was not significantly affected by secondary flows originating near the endwall. Additional heat transfer and film cooling effectiveness results from an endwall and airfoil within an annular low aspect ratio cascade are presented by Sato, et al (1987).

Of work near concave surfaces with injection, Kobayashi (1972,1975), examined the effects of blowing and suction and how they affected the onset of longitudinal vortices in laminar boundary layers. Results showed that suction increases the stability of laminar boundary layers to centrifugal instabilities, whereas blowing had little influence on the instability. El-Hady and Verma (1984), showed that the overall effect of suction or cooling was to stabilize boundary layers by reducing the amplitude ratio of the vortices. Honami and Fukagawa (1987) present velocity, temperature and film effectiveness measured downstream of rows of holes in turbulent flow near flat and concave surfaces. For a blowing ratio of 0.47, concave curvature causes little change in film effectiveness when lateral injection is employed and a significant decrease with streamwise injection. Schwarz and Goldstein (1988) measured local film effectiveness from a row of film cooling jets in turbulent flows near concave surfaces. The authors found that lateral mixing between jets is enhanced as a result of Taylor-Görtler cells at a blowing ratio of 0.4. For m values of 0.8 and 1.6, this mixing and the lateral sway of jets becomes less.

Ligrani, et al (1988) examined the influences of embedded longitudinal vortices on film cooling from a row of holes in turbulent boundary layers. The investigators present surface heat transfer distributions, mean velocities and mean temperatures which show that film coolant is greatly disturbed and local Stanton numbers are altered significantly by the secondary flows within the vortices. Because the character of these secondary flows changes around the vortex, the spanwise position of the vortex with respect to film cooling holes is very important. In addition, secondary heat transfer peaks associated with regions of high streamwise velocity exist which become higher in magnitude and more persistent with downstream distance as the blowing ratio increases from 0.47 to 1.26.

The present study is intended to provide additional understanding of the complex events which occur when longitudinal vortices disturb injectant from film cooling holes. The study is different from other ones where one or two rows of holes are used (Goldstein and Chen, 1985, 1987; Ligrani, et al, 1988; Schwarz and Goldstein, 1988), since only one film cooling hole is employed. Consequently, the interaction between the vortex and injection is clearer because interactions with injectant from neighboring injection holes are not present. Attention is focussed on heat transfer and film-coolant distributions. In particular, the influence of spanwise vortex position with respect to the injection location is investigated for a constant blowing ratio of approximately 0.50. In order to isolate the influence of the vortex only, tests are conducted on a flat plate in a zero pressure gradient. Because prediction of these complex flow interactions is not yet possible, experimental results such as the ones presented here offer designers the best insight into the complex interactions between wall jets and vortices. Understanding such interactions is needed as improved cooling schemes for turbine passages are designed which allow for maximum inlet temperatures and higher efficiencies.

EXPERIMENTAL APPARATUS AND APPROACH

The experiments were conducted in an open-circuit, subsonic wind tunnel located in the laboratories of the Department of Mechanical Engineering at the Naval Postgraduate School. This facility is the same one employed and described by Ligrani, et al (1988). A centrifugal blower is located at the upstream end, followed by a diffuser, a header containing a honeycomb and three screens, and then a 16 to 1 contraction ratio nozzle. The nozzle leads to the test section which is a rectangular duct 3.05 m long and 0.61 m wide, with a topwall having

adjustable height to permit changes in the streamwise pressure gradient.

A schematic is presented in figure 1 showing the locations of the vortex generator, injection hole, and heat transfer surface along the test section.

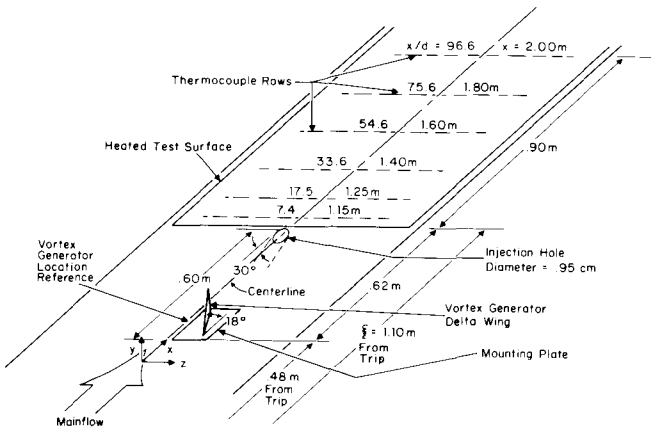

Figure 1. Schematic of test surface including coordinate system.

The coordinate system is also included. Here, z is measured from the tunnel centerline. The leading edge of the vortex generator delta wing is 0.48m downstream of the boundary layer trip. The injection hole is located on the center line and inclined 30 degrees with respect to the horizontal test surface. Its downstream edge is 0.60 meters from the delta wing and 0.02 meters upstream of the constant heat flux test surface. With the heat transfer surface at elevated temperature, an unheated starting length of 1.10 m exists. Freestream air is maintained at ambient temperature, and thus, the direction of heat transfer is from the wall to the gas. Also labelled in figure 1 are the locations of thermocouple rows along the heat transfer surface.

The vortex generator consists of a half-delta wing attached to the wind tunnel floor at an angle of 18° with respect to the tunnel centerline. The height of the wing is 3.0 cm and the base is 7.5 cm. The design is described by Williams (1988) and Ligrani, et al (1988). This configuration produces a vortex at x/d = 41.9 with a circulation to freestream velocity ratio of about -1.10 cm.

The diameter of the centerline injection hole is .952 cm, scaled such that δ_1/d is approximately 0.38. Non-dimensional coolant temperature θ was maintained at approximately 1.5 for all tests. The injection system is described by Ligrani, et al (1988). Air originates in a 10 HP two stage, 150 psig Ingersol-Rand air compressor. From a plenum chamber beneath the test surface, the injectant enters film cooling tubes which extend to the floor of the test section. For the present study, an injection tube on the centerline was used in addition to two other tubes on each side. These two peripheral holes are required to maintain steady flow in the injection system at measurable flow rates. The vortex affects injectant only from the centerline tube; injectant from the two peripheral holes does not touch the heat transfer surface or affect the heat transfer measurements. The experimental uncertainty of the blowing ratio m, based on a 95 percent confidence level, is about 5.0 per cent.

The heat transfer surface was designed and developed to provide a constant heat flux over its area. The plate is constructed so that its upward facing part is adjacent to the wind tunnel air stream, with a thin stainless steel foil surface, 1.3 m x .467 m x .20 mm, painted flat black. Attached to the underside of the foil are 126 copper-constantan thermocouples in six rows. In each of the six rows, 21 thermocouples are located 1.27 cm apart to provide adequate spanwise resolution of temperature distributions. A thin foil heater is used to provide power to the surface. The foil within this heater is custom designed with adjacent braces sufficiently close together to maintain a uniform heat flux boundary condition. For all tests, power levels are adjusted to maintain overall temperature differences less than 30 degrees Centigrade to minimize the influences of variable properties.

To determine the heat loss by conduction from the heat transfer test surface, an energy balance was performed. Radiation losses from the top of the test plate were estimated analytically. The thermal contact resistance between thermocouples and the foil top surface was estimated based on the outputs of the thermocouples and measurements from calibrated liquid crystals on the surface of the foil. Calibrations of the Chameleon encapsulated liquid crystals (manufactured by Appleton Papers Division of the National Cash Register Company) were made to allow foil surface temperatures to be measured within ± 0.3 degrees Centigrade by visual comparison. This uncertainty is included in the determination of overall experimental uncertainties of the Stanton number and Stanton number ratio which are typically about 4.4 and 5.5 percent, respectively.

Calibrated copper-constantan thermocouples were used to measure the free-stream temperature, and injection plenum temperature. For plate temperatures, one calibration was used for all thermocouples of similar manufacture, since their outputs were the same within one or two microvolts at any given temperature. Temperature surveys of ($T - T_\infty$) were performed using two individually calibrated thermocouples, and a two-component automated traversing device. Here, T is the local boundary layer static temperature. As the traverse was made, one thermocouple was placed to measure the freestream temperature as the other was traversed through the boundary layer. Two electric motors manufactured by Superior Electric Co. drove the traverse. These were controlled by a microprocessor operated by a Hewlett-Packard 9836S computer. Each survey consisted of 800 probe locations, covering an area of 12 cm x 22 cm. Free stream and wall temperature

experimental uncertainties are typically .13 and .41 degrees Centigrade, respectively.

Measurements without a vortex and without film cooling were used to qualify the heat transfer plate and measurements procedures employed. Spanwise-averaged Stanton numbers show agreement with the empirical equation from Kays and Crawford (1980) within ± 6 percent. Comparison is made for a turbulent boundary layer on a flat plate at constant freestream velocity, constant heat flux, and an unheated starting length of 1.10 m. Additional details regarding qualification tests and measuring details are given by Ortiz (1987) and by Williams (1988).

The three mean velocity components were measured using a five-hole pressure probe manufactured by United Sensors and Control Corporation. The probe was a conical-type with a diameter of 6.35 mm. Calibration results are given by Williams (1988). The probe was connected to five Celesco model LCVR differential pressures transducers, each with a range of 2.0 cm of water differential pressure. Transducer output signals were converted to DC signals by Celesco CD-10D carrier demodulators. Voltages from the carrier demodulators and thermocouples were read by an HP-3497A Data Acquisition/Control Unit with an HP-3498A Extender. These units were controlled by a Hewlett-Packard Series 300, Model 9836S computer.

The injectant was visualized by contaminating it with atomized liquid droplets in the injection plenum, produced by a Model 1500 Rosco Fog Machine. For these tests, plenum pressure was maintained entirely by the fog machine. Freestream wind tunnel conditions were then set to achieve desired blowing ratios.

BOUNDARY LAYERS WITH FILM COOLING ONLY

Local Stanton number ratios measured with film injectant from the centerline injection hole at m = .53 are presented in figure 2. These are presented as a function of spanwise coordinate z at different x/d.

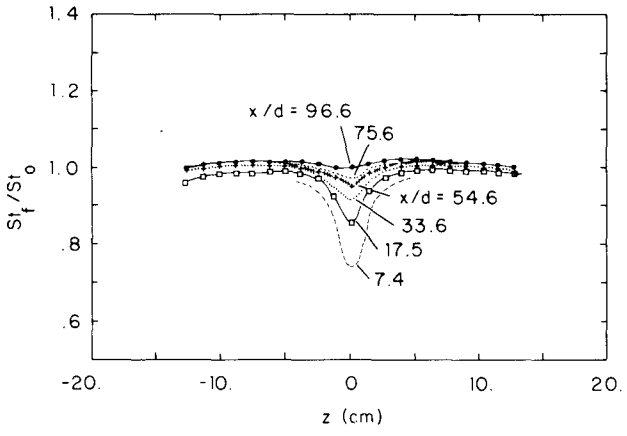

Figure 2. Local Stanton number ratios with film cooling from a single injection hole and no vortex, m = 0.53.

The influence of the coolant is evident where St_f/St_o values are non-unity. This is particularly evident for x/d = 7.4 where ratio values are as low as 0.75. With downstream distance, the Stanton ratios then increase, the protection provided by film cooling becomes less, and the injectant spreads in the lateral direction. These trends are consistent with Goldstein, et al (1968), who studied the behavior of film cooling from a single injection hole inclined at 35 degrees. In that study, adiabatic wall temperatures and adiabatic film cooling effectiveness are used to describe local heat transfer behavior.

The results in figure 2 thus further qualify the experimental procedures and apparatus used to produce injection from a single hole and to measure spatially resolved heat transfer distributions.

VORTEX POSITION WITH RESPECT TO THE INJECTION HOLE

In order to investigate the effect of spanwise position of the vortex, the spanwise location of the vortex generator was changed. The four different spanwise locations used are designated b, e, h and k, and summarized in Table 1. Figure 3 is also presented in order to illustrate the locations of centerline injection with respect to different portions of the vortex.

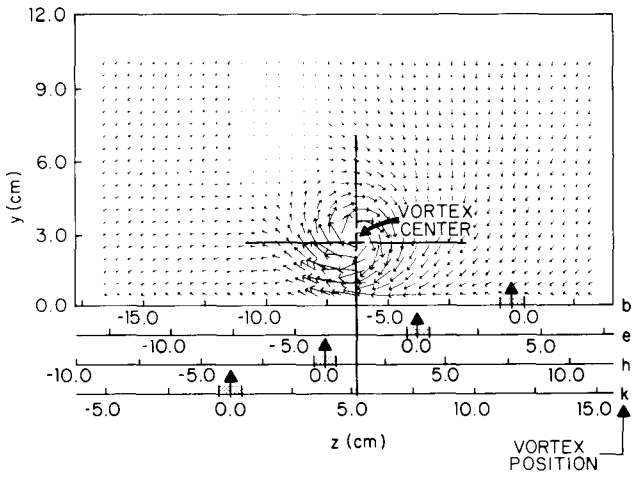

Figure 3. Film cooling injection locations with respect to vortex center and secondary flow vectors for vortex positions b, e, h, and k. Each horizontal scale corresponds to a different vortex position where z = 0 corresponds to centerlines of injection holes.

The secondary flow vectors shown were actually measured just downstream of the injection hole with the vortex at position e. The horizontal axis is then shifted in the figure so that injection centerline location z = 0 is appropriately oriented with respect to the vortex center for each of the four vortex positions. The vortex center is

Table 1. Spanwise locations of the vortex generator, and the vortex at the injection location.

VORTEX POSITION DESIGNATION	VORTEX CENTER Z-LOCATION AT INJECTION LOCATION x/d = 0	INJECTION LOCATION WITH RESPECT TO VORTEX	VORTEX GENERATOR MOUNT Z-LOCATION
b	-6.3 cm	BENEATH DOWNWASH	-3.8
e	-2.5 cm	BENEATH DOWNWASH	0.0
h	1.3 cm	BENEATH CORE AND UPWASH	3.8
k	5.1 cm	TO SIDE OF UPWASH	7.6

located at the peak of the streamwise vorticity.

Of importance here is the location of different positions of the vortex with respect to the injection hole exit. For vortex positions b and e, the vortex center is estimated to be at z = -6.3 cm and z = -2.5 cm, respectively, at the injection location, x/d = 0. In both cases, injectant exits the hole beneath the vortex downwash, but each at a different part of the downwash. For vortex position h, the center of the vortex is located at z = 1.3 cm as it passes over the injection location. In this case, injectant issues just to the side of the vortex center, beneath the core and upwash. For position k, the coolant exits to the side of the vortex upwash when the vortex center is located at a z coordinate value of 5.1 cm.

BOUNDARY LAYERS WITH FILM COOLING AND VORTEX

The effects of an embedded vortex on the film cooled boundary layer are now discussed. This presentation is made in three parts. First, vortex characteristics are discussed. Second, data are presented showing how the vortex alters and redistributes the injectant from the film cooling hole. Third, heat transfer measurements are presented and discussed. For all tests, the freestream velocity is maintained at approximately 10 m/s and spanwise vortex locations b, e, h, and k are employed. The blowing ratio is maintained at 0.50 - 0.53. According to Goldstein et al (1968), these values of m are optimal in regard to the protection provided for injection into a turbulent boundary layer from a single hole inclined at 35 degrees.

Vortex Characteristics

Streamwise velocity contours measured at x/d = 41.9 with an embedded vortex at position e and injection from the centerline hole (z = 0 cm.) are shown in figure 4a. The vortex shows typical characteristics. For z equal to - 8 cm to - 5 cm a secondary flow upwash region is present which results in the convection of low momentum fluid away from the wall. Local boundary layer thickness is greater than its nominal two-dimensional value. The downwash region exists for a z range from - 2 cm to 2 cm. Here, high velocity freestream fluid is brought very close to the wall as evidenced by a very thin boundary layer. These perturbations to local boundary layer behavior by the secondary flow vectors are more responsible than any other effect for heat transfer differences from those measured in a turbulent boundary layer with a two-dimensional mean flow field. A velocity deficit is also present surrounding the vortex center which is located at z = -3.56 cm and y = 2.98 cm. The circulation Γ of this vortex is .133 m^2/sec., a value calculated assuming that all vorticity magnitudes less than 20 percent of the peak vorticity are zero. The ratio Γ/U_∞ is then 1.33 cm. In order to characterize vortex strength relative to injection rate and jet size, the parameter Γ/dU_c is used. For the vortex at x/d = 41.9, the value of this parameter is 2.80.

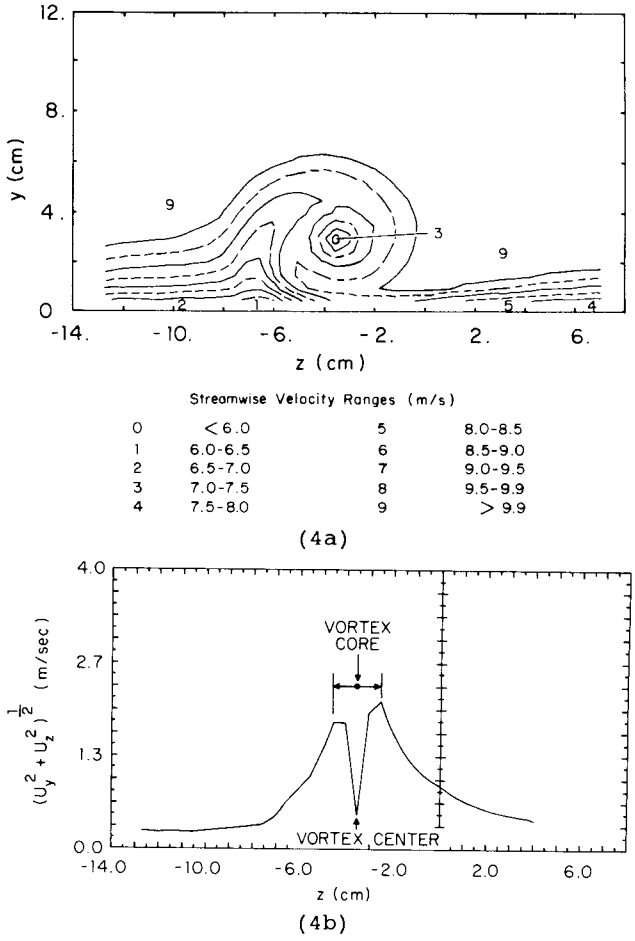

Figure 4. Embedded vortex characteristics at x/d = 41.9, m = 0.5, and vortex at position e. (a) streamwise velocity contours, (b) secondary flow velocity magnitudes at y location of vortex center.

The magnitudes of the secondary flow vectors $(U_y^2 + U_z^2)^{1/2}$ are plotted in figure 4b. These are given for different z locations at a constant y of 2.98 cm, the distance from the wall of the vortex center. The z-location of the center is also indicated along with the region corresponding to the vortex core. The core is an approximately circular region bounded by secondary flow vector maxima, which contains most of the vorticity. For the vortex whose characteristics are shown in figures 4a and 4b, the core is approximately axisymmetric with an average spanwise extent of 2.04 cm., or an average radial extent from the vortex center of 1.02 cm. This average core radius in the lateral direction is designated c. 2c/d, the ratio of spanwise core diameter to hole diameter, is then used to quantify the size of the vortex relative to the injection hole. For the vortex at x/d = 41.9, 2c/d equals 2.14.

When the vortex of figure 4a passes x/d = 0, the center is located at a spanwise position of - 2.5 cm (see Table 1). The injection location is then beneath the vortex downwash. At x/d = 41.9 figures 4a and 4b show the center to be further to the left as a result of spanwise motion of the vortex core in the negative z direction. This is caused by the secondary flow between the core and the wall which are also directed in the negative z direction. Spanwise core motion is also evident from surface Stanton number contours in other studies, particularly those measured downstream of a row of injection holes by Ligrani, et al (1988).

Effects of the vortex on the distributions of film coolant

Information on the disruption imposed to the injectant is evident from flow visualization results presented in figure 5.

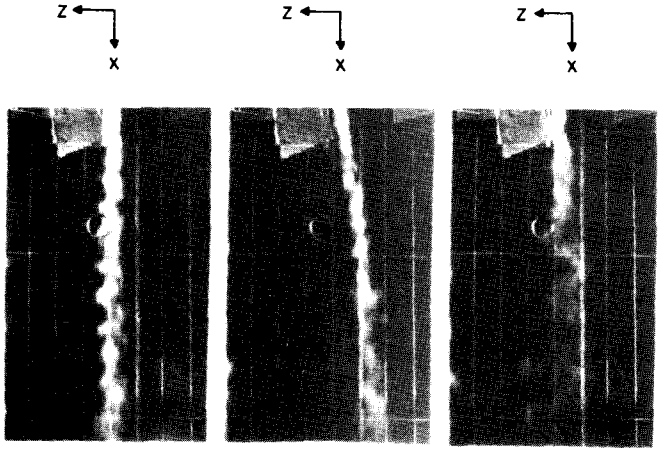

Figure 5. Flow visualization of injectant for m = 0.5. Freestream flow is from top to bottom. (a) no vortex, (b) vortex at position e, (c) vortex at position h.

Horizontal lines in this figure correspond to thermocouple row locations. Vertical lines are 2.54 cm apart starting at the centerline. The longitudinal and spanwise extents of each photograph are approximately 34 and 20 injection hole diameters, respectively. Figure 5a shows the path and behavior of injectant when no vortex is present. Coolant is convected in the x-direction with some spreading with downstream distance. Structures having scales with sizes of the order of the injectant width are present which clearly indicate the turbulent nature of the flow. Results in 5b are for vortex position e when the cooling hole is initially beneath the downwash. Here, considerable deflection from the nominal x-direction is apparent. This results from the rearrangement and distortion imposed by the vortex secondary flow in addition to the spanwise motion of the vortex as it convects downstream. Considerably greater distortion and spreading are apparent in figure 5c. Here, the vortex is located at position h and the injection hole is initially just beside the vortex core beneath the upwash. Some deflection with downstream distance is apparent as coolant is swirled and spread across the vortex by secondary flows. Because much of this spreading is in the positive z direction, coolant seems to be convected into the area away from the wall above the vortex core where secondary flow vectors are also in the positive z direction. This discussed in more detail shortly.

Figure 6 provides quantitative information regarding the distortion and redistribution of injectant by the vortex. The figure is presented in four parts, one for each spanwise vortex position. Measured secondary flow vectors are superimposed on each part to illustrate their significance and influence in regard to redistribution of injectant. Mean temperature fields for each vortex position at x/d = 41.9 are also included in figure 6. These data were obtained using an experimental approach introduced by Ligrani, et al (1988), in which injectant is heated to about 50°C without providing any heat to the test plate. The temperature field is given as $(T-T\infty)$ in degrees Centigrade and thus shows how fluid from the injection hole is convected and distorted by the vortex, where higher temperature differences generally indicate greater amounts of injectant. In cases where higher temperature differences are not from accumulation of injectant by convective processes, they are a result of diffusion or dissipation of heat from fluid which was initially injectant. Thus, one way or another, the temperature variations in figure 6 result from film injection and its interaction with the surrounding flow, since the injectant is the only source of thermal energy (relative to the freestream) for these tests.

A qualitative comparison of figures 6a-6d for vortex positions b,e,h and k shows vastly different injectant distributions with spanwise vortex location. Referring to Table 1 and figure 6a for vortex position b, the downwash part passes over the film cooling hole such that the vortex center is -6.3 cm away in the z-direction. This distance is equivalent to 6.2 core radii or 6.2c. Keeping in mind that the centerline of the

injection hole is located at z = 0, figure 6a indicates that the bulk of the coolant at x/d = 41.9 is at z locations from z = 0 to z = -4.0 cm. This evidences some skewing of coolant from the nominal streamwise

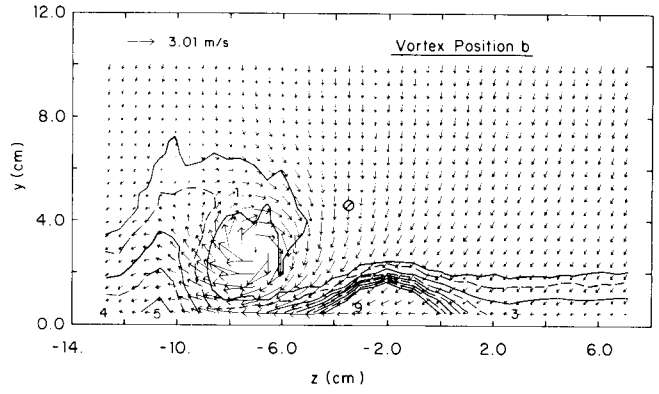

(6a)

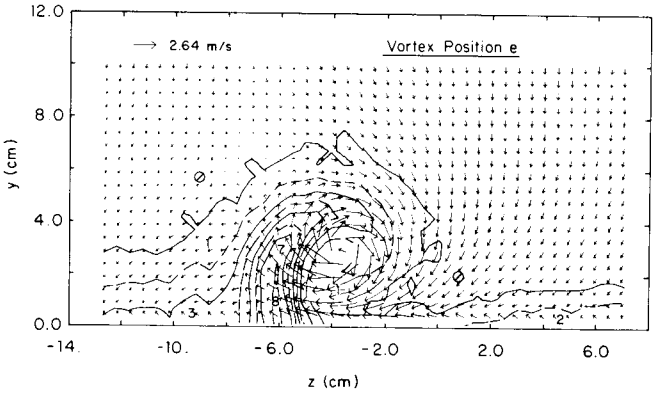

(6b)

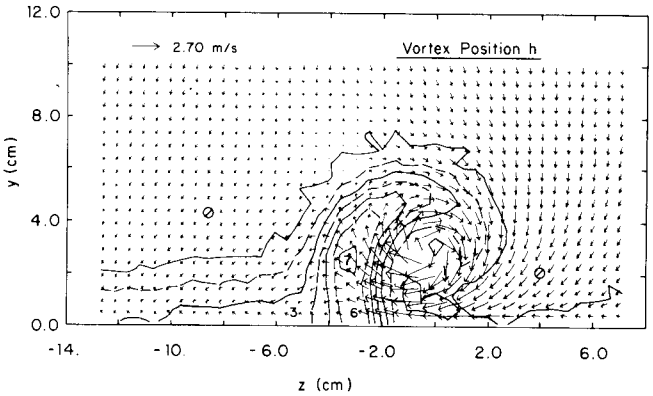

(6c)

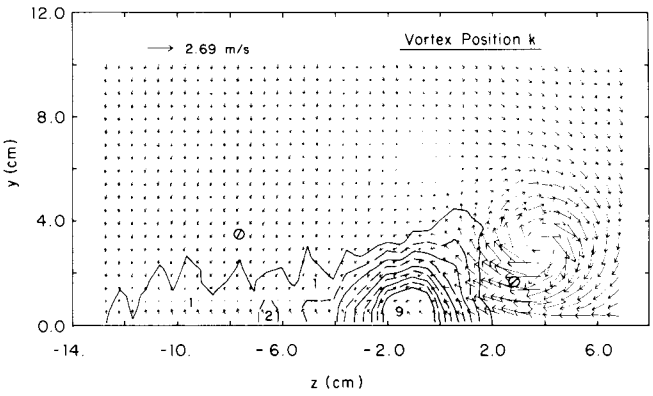

(6d)

$T-T_\infty$ (Degrees Celcius) Ranges

0	< 0.10*	5	1.00-1.25
1	0.10*-0.25	6	1.25-1.50
2	0.25-0.50	7	1.50-1.75
3	0.50-0.75	8	1.75-2.00
4	0.75-1.00	9	> 2.00

*In 5a, this limit is 0.05.

Figure 6. Mean temperature field showing distributions of film coolant with secondary flow vectors at x/d = 41.9, m = 0.5. (a) vortex at position b, (b) vortex at position e, (c) vortex at position h, (d) vortex at position k.

direction. Because of the secondary flow, additional coolant is convected along the wall in the negative z-direction. Some is then distributed away from the wall by the vortex upwash to eventually be swirled around the vortex core. The most significant conclusion from 6a is that the coolant, although skewed from the nominal streamwise direction and partially depleted from secondary flow convection, remains in sufficient quantity to locally protect the surface and minimize heat transfer.

When the vortex is in position e, the injection hole is again beneath the downwash as the vortex passes, but the vortex center is only -2.5 cm or -2.45 c away (Table 1). Figure 6b, again for x/d = 41.9, shows that the coolant is totally redistributed by vortex secondary flows with little local protection remaining near the wall at any spanwise location. Most coolant is located in the vortex upwash region near z = -6 cm, with some above the vortex core. Corresponding streamwise velocity contours in figure 4a show injectant is present at the location of a significant velocity deficit. Such a deficit is typical of the upwash where low momentum fluid is convected away from the wall, however, here the deficit may be slightly augmented due to accumulation of

injectant. Thus, with position e, a significant portion of injectant seems to be initially spread along the wall beneath the vortex center, and then convected in the direction of secondary flows, an observation also consistent with the flow visualization results in figure 5b.

Figure 6c presents coolant distributions and secondary flow vectors at x/d = 41.9 for vortex position h. For this situation, the vortex center was located +1.3 cm or about 1.3 c away from the centerline at x/d = 0 and the injection hole is beneath the vortex core and upwash (Table 1 and Figure 3). As for position e, most of the coolant is redistributed into the upwash region and above the vortex core at this streamwise location. There is little evidence of any significant accumulation of coolant near the wall indicating that most all protection is decimated. A comparison of 6b and 6c shows more significant spanwise spreading for the latter case, a result also seen in the flow visualization photographs in figures 5b and 5c. Such behavior is the likely explanation for the high Stanton number regions observed for some vortex positions by Ligrani, et al (1988) as well as the lateral mixing occasionally noted by Schwarz and Goldstein (1988).

Results in figure 6d are given when the vortex center is located at z = +5.1 cm (or about +5.0 c) as it passes the injection hole. Coolant thus exits the hole to the side of the vortex upwash region. Although some distortion of the coolant distribution seems to result from the vortex upwash, most of it remains intact. Another interesting feature is the spreading of the injectant along the wall which occurred upstream of the x/d = 41.9 location. This seems to have been significant in the negative z direction, however secondary flow vectors beneath the vortex core seem to have prevented significant spreading in the positive z-direction.

Heat transfer results

Spanwise variations of local Stanton numbers for x/d = 33.6 are presented in figure 7.

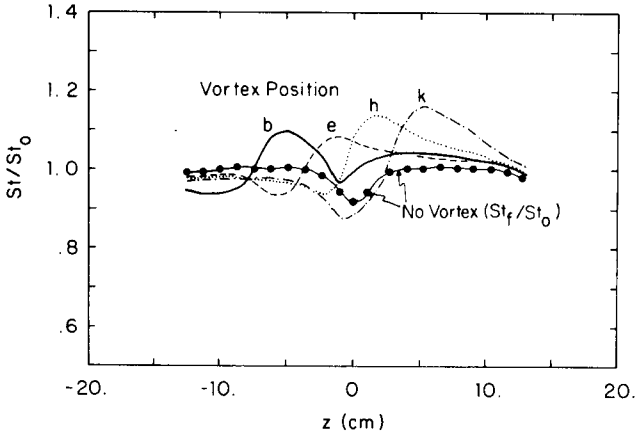

Figure 7. Local Stanton number ratios at x/d = 33.6, x = 1.4 m, m = .51 - .53. Boundary layer with film cooling, with and without an embedded vortex at position b, e, h and k.

These are presented for comparison with the injectant distributions of figure 6 for all four spanwise vortex positions b, e, h, and k. In this figure and the discussion which follows, St_o refers to baseline Stanton numbers without a vortex and without film cooling, St_f are measured with film cooling only, and St are obtained with vortex and film cooling.

The most important features of figure 7 are the differences between the St/St_o distributions and the St_f/St_o curve for no vortex. This illustrates the significance of the perturbation caused by the vortex to the film cooled boundary layer. Also of importance are the changes of the St/St_o distributions and magnitudes which occur as the spanwise position of the vortex is changed. Such alterations evidence the complexity of the interactions between the injectant, the vortex, and the boundary layer.

Without the vortex present, St_f/St_o shows a deficit of approximately 0.92 at z = 0 resulting from the injectant. Similar deficits when vortices are present evidence presence of injectant and the amount of protection that is provided. Ordinarily, without an externatal perturbation, an embedded vortex produces spanwise Stanton numbers which are augmented near the downwash side and diminished near the upwash side. In the figure 7 view looking downstream, the downwash is on the right and the upwash is on the left for each vortex position. With injectant present, upwash and downwash St/St_o are further altered depending upon the location of the injectant with respect to these regions.

With vortex position b, figure 6a shows the presence of injectant near the wall at the exact location that a local deficit exits on figure 7 for vortex position b: -4.0 cm < z < 0.0 cm. Similar deficits are not present near z = 0 cm in figure 7 for vortex positions e and h. For both cases, coolant is swept away from the wall into the upwash and above the vortex core by secondary motion. Consequently, little evidence of lowered St/St_o from the presence of injectant is seen for these vortex positions, except that the St/St_o peak for position e is slightly lower than for other vortex positions. For vortex position k, St/St_o values are lower than St_f/St_o data with film cooling only. Thus, the protection provided by the injectant seems to be locally augmented by the vortex for -5 cm < z < 3 cm. This protection also appears to be spread over a larger portion of the wall as a result of near-wall secondary motion in the negative z direction.

The streamwise development of St/St_o and St_f/St_o distributions for vortex positions b, e, h and k are given in figures 8, 9, 10, and 11, respectively. Close inspection of these figures, as well as figures 6 and 7, reveals vortex positions to be slightly different from the ones produced by the repositioning of the vortex generator alone. This is because of interactions with injection jets which produce small alterations to the y and z locations of the

vortex center as well as the vortex path as it convects downstream.

Referring to figure 8 for vortex position b for x/d = 7.4, significant influence of the injectant is indicated by St/St_o values which are as low as ones without a vortex present. For smaller values of z, regions where $St/St_o > St_f/St_o$ and $St/St_o < St_f/St_o$ correspond to the downwash and upwash portions of the vortex, respectively. At x/d = 7.4, high St/St_o from the vortex downwash are just to the left of St/St_o deficits from the film injectant.

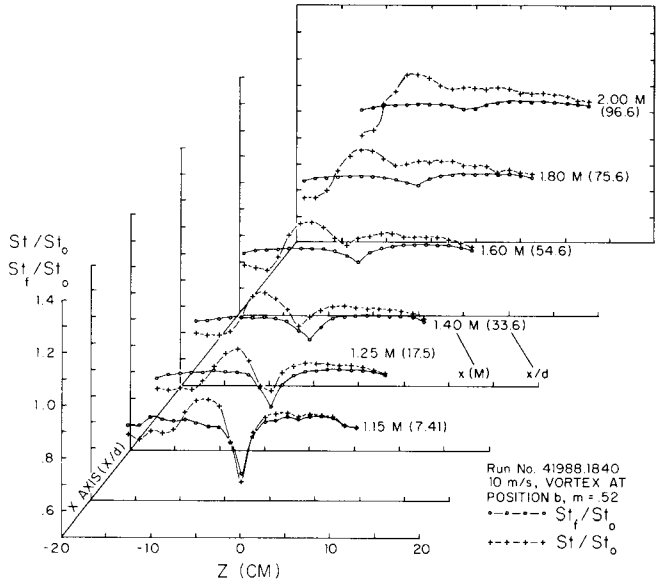

Figure 8. Local Stanton number ratios. Boundary layer with film cooling, with and without embedded vortex.

With downstream development, the influence of injectant on the St/St_o data is evident for x/d up to 54.6. As x/d increases over this range, Stanton number ratio deficits associated with film cooling near z/d = 0 become less apparent. Corresponding St/St_o are also higher than those obtained without the vortex. This occurs as increasing amounts of injectant are swept away from the wall into the upwash and less coolant is available near the wall to reduce heat transfer. Such behavior is consistent with high St/St_o attributable to the downwash which persist to the end of the test plate, as well as the secondary flow motion and injectant distributions presented in figure 6a. Because of the coherence of the vortices, their perturbations to heat transfer persist at least 97 injection hole diameters downstream, a result also observed by Ligrani, et al (1988).

With vortex position e in figure 9, a significant St/St_o valley attributable to film injection exists at x/d = 7.4. Here the vortex is probably just lifted off the surface by the injectant. With further downstream development (x/d ≥ 17.5), the direct application of the vortex downwash

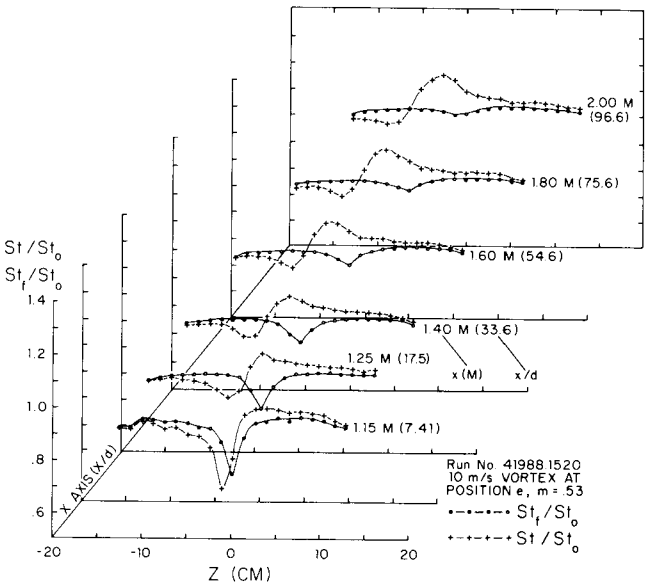

Figure 9. Local Stanton number ratios. Boundary layer with film cooling, with and without an embedded vortex.

begins to take its toll on the region containing the injectant. High St/St_o from the vortex downwash are at the same spanwise locations as St_f/St_o minima from film cooling. Consequently, little evidence of injectant is evident except that maximum and minimum St/St_o at each streamwise location are both slightly less than if no film cooling is present. The protective influence of the film cooling thus appears to be almost totally decimated, as evidenced by the St/St_o peak near z/d = 0 which persists to the end of the test plate.

Similar conclusions may be drawn regarding the St/St_o data for vortex position h in figure 10. Only when x/d equals 7.4 and 17.5 are local minima St/St_o slightly modified by the injectant. Here, St/St_o maxima corresponding to the vortex downwash are just to the right of St/St_o deficts from film injection. At other locations, the spanwise variations of St/St_o primarily reflect the influence of the vortex only.

With vortex position k, injectant emerges from the cooling hole to the side of the upwash. Consequently, St/St_o deficits from film injection are at smaller z than St/St_o peaks from vortex downwash regions. This is evident in figure 11, which also shows that evidence of injectant is seen for x/d at least up to 54.6. In addition, minima St/St_o are lower than St_f/St_o with cooling only. This results from the combined influence of the downwash and the injection, as well as interactions between the two. Thus, over considerable downstream distances, the protection provided by film cooling is locally augmented and spread over a larger area than if no vortex is present. Similar observations were made by Ligrani, et al

(1988) for vortex upwash near a row of holes.

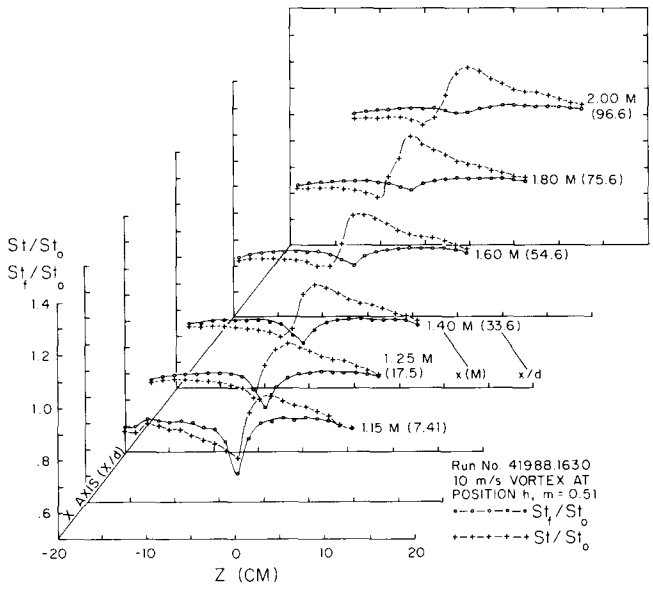

Figure 10. Local Stanton number ratios. Boundary layer with film cooling, with and without an embedded vortex.

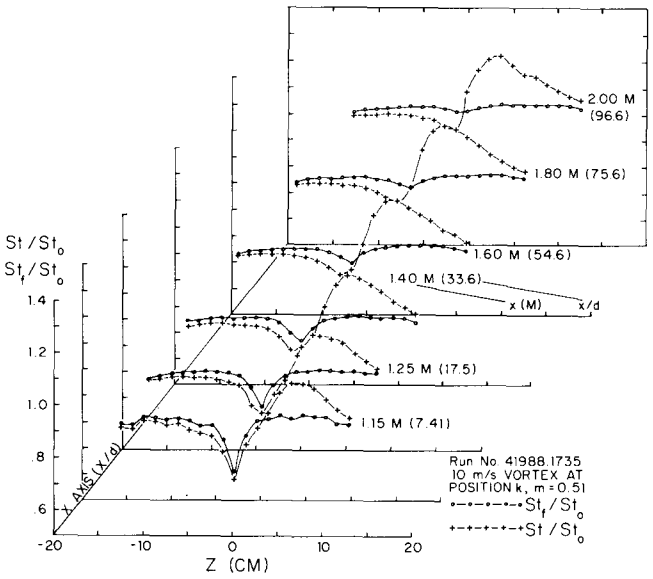

Figure 11. Local Stanton number ratios. Boundary layer with film cooling, with and without an embedded vortex.

SUMMARY AND CONCLUSIONS

The interaction and effect of a single embedded vortex on injectant from a single film cooling hole inclined at 30 degrees was investigated. All measurements were made with a blowing ratio of approximately 0.50 and a freestream velocity of 10 m/sec. At x/d = 41.9, the circulation and core diameter of the vortices employed were about .133 m^2/sec. and 2.04 cm., respectively. These give a ratio of core diameter to injection hole diameter 2c/d of 2.14, and ratio of circulation to injection velocity times hole diameter $\Gamma/U_c d$ of about 2.8.

Four spanwise vortex positions with respect to the film cooling hole were used to examine the interactions of different parts of the vortex on the injectant. The most important general conclusion is that injectant continues to provide near-wall protection if it is located at least 2.0 - 2.5 core diameters away from the vortex center in the spanwise direction as the vortex passes. However, regardless of the vortex position with respect to injection location, the vortices produce perturbations to local heat transfer distributions, including local maxima, which persist as far as 97 hole diameters downstream of the injection location. When injectant issues directly beneath the vortex downwash, magnitudes of these maxima are somewhat reduced compared to other vortex positions.

More specific conclusions follow.

(1) When the vortex center passes the injection hole within 1.2 diameters on the downwash side and within 0.6 diameters on the upwash side (vortex positions e and h, respectively), most injectant is swept beneath the core and into the upwash away from the wall by secondary flows. In these cases, little protection from film cooling remains since local Stanton numbers deficits are present for x/d of 7.4 but not for x/d $\geq$ 17.5. When the vortex downwash passes immediately above the injection location (vortex position e), Stanton number peaks are slightly lower then if no injectant were present.

(2) When the injectant emerges beneath the downwash 3.1 core diameters from the center (vortex position b), Stanton numbers are influenced by the coolant for x/d up to 76. Even though injectant is skewed from the streamwise direction and is partially depleted by secondary flow convection, it remains in sufficient quantity to minimize heat transfer locally.

(3) When injectant leaves the cooling hole on the upwash side 2.5 core diameters from the vortex center (vortex position k), local Stanton number distributions show local deficits from film cooling for x/d at least up to 54.6. In this case, the local protection provided by film cooling seems to be augmented by the presence of the vortex. In addition, the area of protection is increased as the injectant is spread over the surface in the direction of near wall secondary flows.

ACKNOWLEDGEMENTS

This study was supported by the Aero-Propulsion Laboratory of Wright Patterson Air Force Base, MIPR Number FY 1455-88-N0608. Dr. Dick Rivir was program monitor. Some of

the facilities used were purchased using funds from the Naval Postgraduate School Foundation Research Program.

REFERENCES

Blair, M.F., 1974, "An Experimental Study of Heat Transfer and Film Cooling on Large-Scale Turbine Endwalls," ASME Transactions-Journal of Heat Transfer, Vol. 96, pp. 524-529.

El-Hady, N.M. and Verma, A.K., 1984, "Instability of Compressible Boundary Layers Along Curved Walls with Suction or Cooling," AIAA Journal, Vol. 22, No. 2, pp. 206-213.

Goldstein, R.J. and Chen, H.P., 1985, "Film Cooling on a Gas Turbine Blade Near the Endwall," ASME Transactions-Journal of Engineering for Gas Turbines and Power, Vol. 107, pp. 117-122.

Goldstein, R.J. and Chen, H.P., 1987, "Film Cooling of a Turbine Blade with Injection Through Two Rows of Holes in the Near-Endwall Region," The American Society of Mechanical Engineers, Paper No. 87-GT-196, pp. 1-7.

Goldstein, R.J., Eckert, E.R.G. and Ramsey, J.W., 1968, "Film Cooling with Injection Through Holes: Adiabatic Wall Temperatures Downstream of a Circular Hole," ASME Transactions - Journal of Engineering for Power, Vol. 90, No. 4, pp. 384-395.

Honami, S. and Fukagawa, M., 1987, "A study on Film Cooling Behavior of a Cooling Jet Over a Concave Surface," Paper 87-Tokyo-IGTC-72, Tokyo International Gas Turbine Congress, Tokyo, Japan.

Kays, W.M. and Crawford, M.E., 1980, Convective Heat and Mass Transfer, Second Edition, McGraw-Hill Book Company.

Kobayashi, R., 1972, "Note on the Stability of a Boundary Layer on a Concave Wall with Suction," Journal of Fluid Mechanics, Vol. 52, pp. 269-272.

Kobayashi, R., 1984, "Taylor-Gortler Instability of a Boundary Layer with Suction or Blowing," Report Institute of High Speed Mechanics, Vol. 32, Series B, pp. 129-148.

Ligrani, P.M., Ortiz, A., Joseph, S.L., and Evans, D.L., 1988, "Effects of Embedded Vortices on Film-Cooled Turbulent Boundary Layers," Paper 88-GT-170, ASME Gas Turbine and Aeroengine Congress and Exposition, Amsterdam, The Netherlands.

Ortiz, A., 1987, "The Thermal Behavior of Film Cooled Turbulent Boundary Layers as Affected by Longitudinal Vortices," M.E. Thesis, U.S. Naval Postgraduate School, Monterey, CA.

Sato, T., Aoki, S., Takeishi, K. and Matsuura, M., 1987, "Effect of Three-Dimensional Flow Field on Heat Transfer Problems of a Low Aspect Ratio Turbine Nozzle," Takasago Research and Development Center, Mitsubishi Heavy Industries, Ltd.

Schwarz, S.G. and Goldstein, R.J., 1988, "The Two-Dimensional Behavior of Film Cooling Jets on Concave Surfaces," Paper 88-GT-161, ASME Gas Turbine and Aeroengine Congress and Exposition, Amsterdam, The Netherlands.

Williams, W.W., 1988, "Effects of an Embedded Vortex on a Single Film-Cooling Jet in a Turbulent Boundary Layer," M.S. Thesis, Department of Mechanical Engineering, Naval Postgraduate School, Monterey, CA.